Elucidating the Mechanism for the Reaction of o-phthalaldehyde with Primary Amines in the Presence of Thiols

Grazia Rovelli[a] and Kevin R. Wilson [a,*]

[a] Chemical Sciences Division, Lawrence Berkeley National Laboratory, Berkeley, 94720, CA, USA

Abstract

The use of o-phthalaldehyde (OPA) in combination with a thiol reagent is a common method for detecting primary amines in amino acids, peptides and proteins. Despite its widespread use, the exact reaction mechanism has been debated since the 1980s. Here we measure the kinetics of the reaction between OPA, alanine and a dithiol (1,4-dithiolthreitol, DTT) as a function of pH and reagent concentration. Using these new measurements and accompanying kinetic model, we find evidence that the pH dependence of the kinetics arises from both the protonation state of alanine and DTT, the hydration state of OPA and the unproductive equilibrium with DTT, all of which are pH-dependent. These results support the mechanism originally proposed by Sternson *et al.* (*Anal. Biochem.*, **1985**, *144*, 233-246) and Wong *et al.* (*J. Am. Chem. Soc.*, **1985**, *107*, 6421-6422), in which the primary amine first reacts with OPA followed by a reaction with the thiol to form the fluorescent isoindole product.

*Correspondence to krwilson@lbl.gov

1. Introduction

The reaction between o-phthalaldehyde (OPA) and a primary amine in presence of a thiol reagent was first reported by Roth[5] in 1971. The product of this reaction is strongly fluorescent, enabling the selective and highly sensitive[6] quantification of primary amines in aqueous solutions of amino acids, peptides and proteins. For these reasons, it is routinely used, commercially available (e.g., Fluoraldehyde™, Thermofisher), and utilized in numerous analytical applications, for example in pre- or post- column derivatization in chromatography[7, 8] or in capillary electrophoresis.[9] Although the fluorescent product was identified as a l-alkylthio-2-alkyl-substituted isoindole,[10] the mechanism for its formation remains unclear.[7, 11]

Two main reaction mechanisms are proposed in the literature. Sternson *et al.*[1] and Wong *et al.*[2] proposed the mechanism shown in Fig. 1A (herein termed the 'Sternson-Wong mechanism'), which first involves the reaction of OPA with a primary amine, followed by the addition of the thiol to form the fluorescent product. Both Sternson *et al.* [1] and Wong *et al.*[2] suggest that there exists a non-productive equilibrium between OPA and the thiol, which does not lead to the formation of the fluorescent isoindole. Alternatively, the mechanism proposed by Simons and Johnson[3] with additional support from Trepman and Chen[12] (Fig. 1B herein termed the 'Simons-Johnson mechanism') suggests that the thiol reacts first with OPA and that the amine is added later to the OPA-thiol intermediate in a final reaction step. An important clue to the mechanism is the strong dependence of the reaction rate on the solution pH. For the reaction of OPA with mercaptoethanol and alanine,[12] the measured pseudo-first-order rate constant increases with pH, reaching a maximum between pH 10 and 11, and then decreasing at pH > 11.

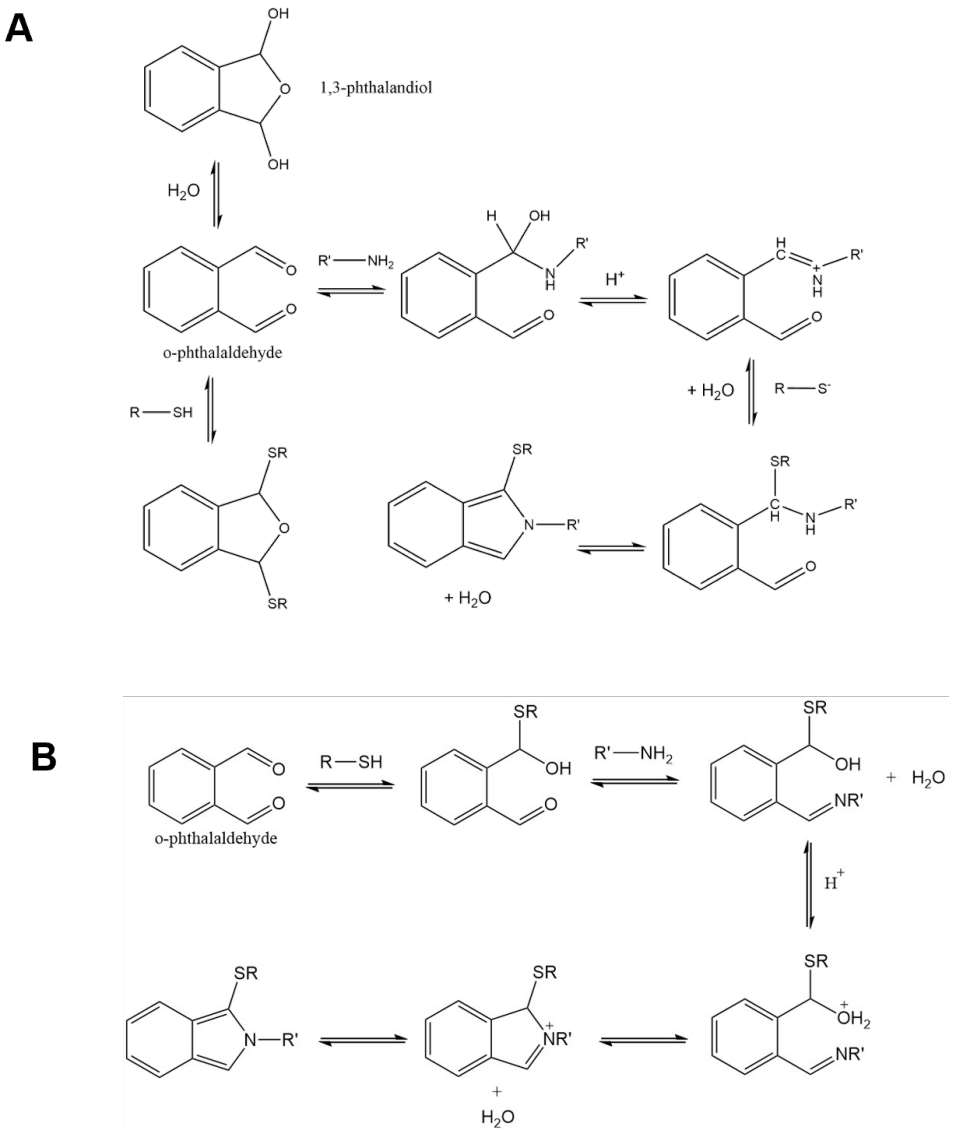

Figure 1: (A) Sternson-Wong mechanism.[1, 2] (B) Simons-Johnson mechanism.[3]

As discussed previously,[7, 11, 13] potential reaction mechanisms reported in the literature are mainly based on the identification of products rather than on kinetic studies. Although product identification has provided valuable insight about the chemical nature of the fluorescent product, to date it has not led to conclusive evidence for the actual reaction mechanism.

Recently, it was observed that the kinetics of the reaction between OPA, alanine and a dithiol (1,4-dithiolthreitol, DTT) are accelerated by ~25% in ~30 μm radius aqueous microdroplets, relative to the same reaction conducted in macroscopic container.[4] The acceleration mechanism(s) of reactions in confined environments remains uncertain, and in charged microdroplets (such as those used in the experiments by Jacobs *et al.*[4] and others[14]) acceleration could originate from the preferential partitioning of reagents to the droplet surface, partial solvation of reagents, altered chemical equilibria at the surface,[15, 16] radial inhomogeneity of reagent concentrations or pH,[17, 18] and the effects of surficial charge and electric fields.[19] Thus, an in-depth knowledge of the OPA-alanine-DTT reaction mechanism would enable greater insight into the nature of the reaction acceleration observed by Jacobs *et al.*[4] as will be detailed in a forthcoming publication.

Here we report a comprehensive study of the reaction kinetics of OPA, alanine and DTT. To interpret the experimental results a kinetic model is developed, with the goal of testing the kinetic viability of previously proposed reaction mechanisms. The reaction rate is measured as a function of pH (at fixed reagent concentrations) as well as a function of excess alanine at pH 9 and 12. Two kinetic models are formulated, one based on the Sternson-Wong mechanism (Fig. 1A) and the other using the Simons-Johnson mechanism (Fig. 1B). To make the model physically realistic, equilibrium and rate constants used in the simulations are constrained by measurements or literature values. The reaction pathways that are considered in the model are selected to account for the products detected by Jacobs *et al.*[4] Finally, we evaluate the predictive capabilities of each model using our concentration-dependent data as well as the kinetics measurements reported by Trepman and Chen[12] and Wong and coworkers.[1, 2] We find that the Sternson-Wong mechanism best replicates both our experimental data and prior kinetics measurement reported in the literature.

2. Methods: Model Formulation

The main challenge in building a kinetic model of the OPA-alanine-DTT reaction is that it involves several coupled and pH-dependent equilibria. These are: 1) the protonation/deprotonation equilibrium of the primary amine, 2) the hydration equilibrium of OPA, 3) the OPA-alanine equilibrium, 4) the OPA-thiol equilibrium, and 5) the protonation/deprotonation equilibrium of the thiol groups in DTT. To realistically include all of these in a kinetic model, the equilibrium constants for each are required, as well as the rate coefficients for the forward and backward reaction steps that comprise the equilibrium constant. It remains somewhat unclear if the formation of the isoindole product is actually an equilibrium, so for simplicity, we assume its formation is non-reversible. Furthermore, it was suggested that the fluorescent product might undergo degradation via several pathways, for example in presence of a large excess of OPA relative to the primary amine.[20] To avoid this complication, OPA is always the limiting reagent in our studies. In the model we do not include any additional degradation pathways and find no evidence for product degradation (e.g., photolysis) that occurs on the timescales of a typical experiment (from > 1 s to ~5 minutes). Below, we outline the model, discuss how rate coefficients are obtained or estimated, as well as a number of chemically-based assumptions that are required in order to accurately predict our kinetic measurements.

Table S1 shows the elementary steps used in the simulation of the Sternson-Wong mechanism, which are also shown in Fig. 2. The major pathways shown in Fig. 2 and included in our model are based upon the products (shown in red) detected by Jacobs *et al.*[4] The kinetic model is expressed as a system of ordinary differential equations (ODE), which are solved as an initial value problem using a Python ODE solver (scipy.integrate.solve_ivp, method 'Radau'). The differential equations are shown in the Supplementary Information (Section S1). The initial concentrations of all chemical species are calculated from the starting concentrations of OPA, DTT and alanine and

we assume that all species are at equilibrium at the beginning of the reaction. The elementary steps and differential equations for the Simons-Johnson mechanism are shown in Section S2. Below we discuss in detail the constraints and assumptions used in the formulation of this model.

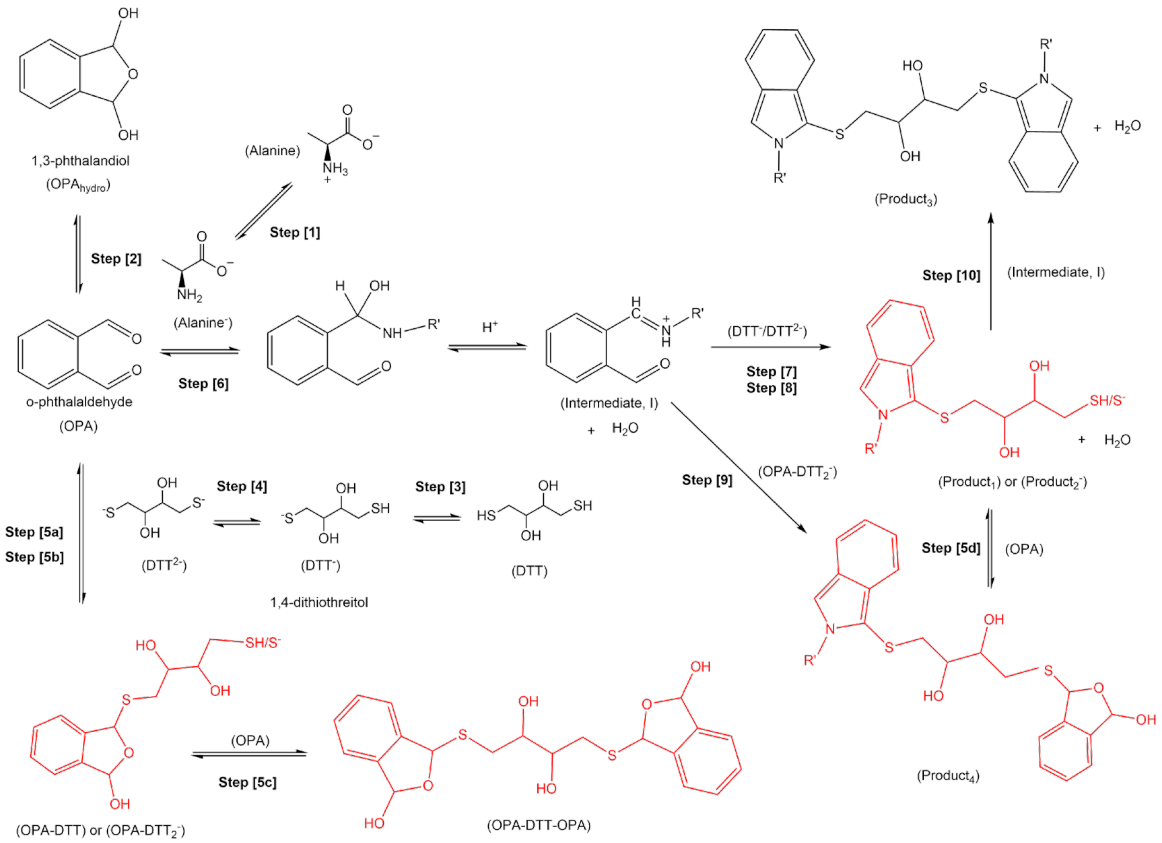

Figure 2: The reaction steps and molecular structures (see Table 1) based on the Sternson-Wong mechanism that describe the reaction between OPA, alanine and DTT. The products shown in red were previously identified by Jacobs et al.[4]

2.1 Alanine protonation/deprotonation equilibrium

There is an indication that it is the deprotonated primary amino group that reacts with OPA.[13] This alanine protonation/deprotonation equilibrium is shown as step 1 in Table S1 and Fig. 2. The ratio of deprotonated/protonated species as a function of pH is calculated from the second pK_a of alanine (9.69) using the Henderson-Hasselbach equation:

$$pH = pK_a + log_{10}([Alanine^-]/[Alanine]) \quad (1)$$

rearranged as:

$$K_a = [Alanine^-]/[Alanine] = 10^{(pH-pK_a)} \quad (2)$$

where $Alanine$ is the zwitterionic form and $Alanine^-$ is the deprotonated form of the amino acid that reacts with OPA. Considering that $K_a = k_{ala_f}/k_{ala_b}$, we constrain the deprotonation rate (k_{ala_f}) to K_a using a diffusion-limited protonation rate (k_{ala_b}) of 10^{10} s^{-1}.[21]

2.2 OPA hydration equilibrium

In aqueous solutions, OPA can exist as non-hydrated, monohydrated and hydrated cyclic hemiacetal forms,[22] as shown in Figure 3. Only the non-hydrated form of OPA (Figure 3A) is believed to undergo the full reaction mechanism to form isoindole.[20] This is because the formation

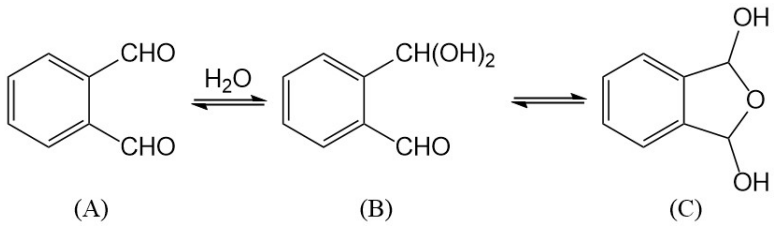

Figure 3: non-hydrated (A), monohydrated (B) and cyclic hemiacetal (C) forms of OPA in aqueous solutions.

of isoindole requires two available carbonyl groups as illustrated in Fig 1. The first carbonyl group reacts with either the amino acid (Sternson-Wong mechanism, Fig. 1A) or the thiol (Simons-Johnson mechanism, Fig. 1B), while the second carbonyl group, in the Sternson-Wong mechanism, is involved in a nucleophilic attack of a subsequent intermediate prior to the formation of isoindole as shown in Fig. 1A and in Ref. [20] For the Simons-Johnson mechanism (Fig. 1B) the reaction of the second carbonyl group with the amine group is required to form isoindole.

Both the hydration equilibrium constants and the hydration/dehydration rate constants of OPA are pH-dependent[22] and are constrained in our model as follows. Since prior literature lacks detailed information on the pH-dependent equilibrium and rate constants for the two equilibria depicted in Figure 3, here we do not discriminate between the two possible hydrated forms of OPA (monohydrated form (B) and cyclic hemiacetal form (C) in Fig. 3), but rather we group those two together into a single hydrated and unreactive species ($OPA_{hydrated}$, step 2 in Table S1). The equilibrium constant, K_{hydro}, is measured spectroscopically as described in Section 3.2. The base-catalyzed pH-dependent rate of dehydration (k_{hydro_f}) was measured by Salem *et al.*,[22] and is found to be proportional to $[OH^-]$ up to a pH of 10.5. Here we expand that linear dependence of k_{hydro_b} vs. $[OH^-]$ to pH values up to 12.5 and constrain the rate of hydration (k_{hydro_f}) using $K_{hydro} = k_{hydro_f}/k_{hydro_b}$. It is worth noting that Salem *et al.*[22] indicated that all three OPA forms can undergo reactions with OH^-, but due to the lack of detailed information on the equilibrium and rate constants for each of these reactions, we have not included these as explicit steps in our model. This approximation is reasonable because by constraining step 2 in our model to the spectroscopic measurements discussed in Section 3.2, we effectively account for the overall quantity of OPA that is 'non-reactive', either due to its hydration state or due to its reaction with OH^-.

2.3 DTT protonation/deprotonation equilibrium

Wong *et al.*[2] suggested that thiolate is more effective at trapping the OPA-alanine intermediate (I, Fig. 2 and Table S1) than the corresponding thiol, which is consistent with S^- being a better nucleophile than SH. The mechanism proposed by Sternson *et al.*[1] also suggests that S^- reacts with the positively charged OPA-alanine intermediate. Thus, we include the single and double deprotonation states of DTT, DTT^- ($pK_{a,1}$ = 9.2) and DTT^{2-} ($pK_{a,2}$ = 10.1) as steps 3 and 4 in Table S1 and Fig. 2. In our model only DTT^- and DTT^{2-} are allowed to react with the OPA-alanine intermediate (I) in Steps 7 and 8 in Table S1 and Fig. 2. OPA-DTT_2^- and $Product_2^-$ both have available $-S^-$ groups, which can react with the OPA-alanine intermediate (I) in Steps 9 and 10 to form $Product_4$ and $Product_3$, respectively. The underlying assumption is that the protonation state of an unreacted SH or S^- group does not change during these reactions. We also assume in the absence of prior literature data that the rate coefficient for these thiolate reactions shown in Steps 7-10 are the same and not influenced by either the protonation state of the second thiol group in DTT or the presence of a covalent bond to an OPA molecule (OPA-DTT_2^-) or isoindole group ($Product_2^-$).

2.4 OPA-DTT equilibrium

Wong *et al.*[2] and Sternson *et al.*[1] suggest that the equilibrium between OPA and the thiol occurs but is unproductive (i.e., does not form the final isoindole product). This equilibrium is included in our model as step 5 in Table S1. There are two thiol groups on each DTT molecule, so we have included the single (Steps 5 a and b) and the double addition (Step 5c) of OPA to DTT, to account for OPA-DTT-OPA species detected by Jacobs *et al.*[4] using mass spectrometry. $Product_2^-$ also has an available thiolate group and can react with OPA in Step 5d to form $Product_4$, also detected by Jacobs *et al.*[4] It is assumed that the equilibrium constants for Steps 5a-d are

identical and are constrained in the model to the equilibrium constant for OPA + DTT (i.e, $K_{eq(OPA\text{-}DTT)}$) measured as a function of pH as described in Section 3.3. No information is available in the literature on the reaction kinetics for the formation of this equilibrium, so in our simulations we varied the magnitude of $k_{OPA\text{-}DTT_f}$ and $k_{OPA\text{-}DTT_b}$ to best replicate our experimental results. We do however constrain the values of $k_{OPA\text{-}DTT_f}$ and $k_{OPA\text{-}DTT_b}$ to be consistent with the values of $K_{eq(OPA\text{-}DTT)} = k_{OPA\text{-}DTT_f}/k_{OPA\text{-}DTT_b}$ measured in Section 3.3.

2.5 Formation of the OPA-alanine intermediate and the isoindole product

Using a simple kinetic model of their experimental data, Wong *et al.*[2, 23] reported rate constants (k_{i_f}) for the formation of the OPA-alanine intermediate (labeled I in Figure 3) of 113 ± 4 M^{-1} s^{-1} and 127 ± 13 M^{-1} s^{-1}. Unfortunately, we are unable to replicate our experimental results using these values. Instead, this rate coefficient is left as an adjustable parameter in the model. To best replicate the overall pH dependence of the reaction (as will be shown below in Section 4) a best fit value of k_{i_f}= 4000 M^{-1} s^{-1} is obtained (step 6 in Table 1). The origin of this discrepancy between the k_{i_f} obtained here and previously by Wong *et al.*[2, 23] is currently unclear, but could be due to the lack of chemical speciation of OPA, alanine, and the thiol in the kinetic analysis used by Wong *et al.*, or the much higher ionic strength ([NaCl] = 4.6 M) used in our kinetic measurements (see Section 3.1).

The backwards rate constant for the dissociation of the OPA-alanine intermediate (k_{i_b}, step 6 in Table S1) and the rate constant for its reaction with DTT^- and DTT^{2-} (k_{prod}, steps 7 and 8 in Table S1) are also left as adjustable parameters in our model. Since DTT^{2-} contains two thiolate groups, two possible fluorescent isoindole products can be formed with either one or two of the S^- groups in DTT reacting with intermediate I (see $Product_2$ and $Product_3$ in Figure 2). It is assumed

that the formation of $Product_3$ takes place in two consecutive steps (steps 7 and 8 in Fig. 2 and Table S1) and that the rate coefficients for the formation of $Product_1$ and $Product_2$ are the same (k_{prod}).

The simplified kinetic analysis reported by Wong *et al.*[2] did not allow them to individually determine k_{i_b} and k_{prod}, but rather only their ratio (i.e., k_{i_b}/k_{prod}). The ratio was determined to be 0.053±0.005 mM and 0.100±0.021 mM for the reaction of the OPA-alanine intermediate with mercaptoethanol and 3-mercatopropionic acid, respectively. The best fit values for $k_{i,b}$ and k_{prod} obtained in our model are 0.057 s^{-1} and $1.1 \cdot 10^3$ M^{-1} s^{-1}, respectively. The ratio of k_{i_b}/k_{prod} is 0.052 mM, which is in agreement with Wong *et al.*[2]

3. Experimental Methods

3.1 Measurements of reaction kinetics

Aqueous solutions of OPA, DTT and alanine were prepared in a 50 mM borate buffer, in presence of 4.6 M NaCl, in order to closely replicate the experimental conditions and ionic strength for the droplet experiments reported by Jacobs *et al.*[4] The pH was adjusted by adding NaOH. No effect on the reaction kinetics in presence of different buffers was observed[13] and we assume that the high ionic strength of our solutions does not substantially affect the overall reaction mechanism. All reagents were purchased from Sigma-Aldrich (OPA: P1378, ≥ 97%; l-alanine: 05129, ≥ 98.5%; DTT: D0632, ≥ 98%; boric acid: 0394, ≥ 99.5%; sodium tetraborate: 221732, 99%; NaCl: S7653, ≥ 99.5%, NaOH: S5881, ≥98%).

Kinetic measurements are initiated by vigorously pipetting 0.8 mL of the alanine solution into 0.8 mL of the OPA/ DTT solution residing in a 3.5 mL cuvette. Once the solutions are mixed the cuvette is continuously stirred during the reaction using a magnetic stir bar. A 355 nm laser (JDS

Uniphase PowerChip NanoLaser) is used to excite the fluorescence of the isoindole product. The time evolution of the fluorescence signal is recorded using a CMOS camera (Thorlabs, DCC1645C). Figure S1 shows a typical fluorescence intensity profile observed across the cuvette. The fluorescence signal is larger at the edge of cuvette where the laser enters, and then decreases indicating that the product is strongly absorbing, and the intensity of the incoming laser light is attenuated across the cuvette. For this reason, the signal at the edge of the cuvette (which corresponds to the maximum in each intensity profile) as a function of time (Fig. 4) is used to monitor the kinetics. The measured fluorescence vs. time is fit to an exponential function ($y = A \cdot (1 - e^{-k_{obs} \cdot x})$) that passes through the origin to obtain k_{obs}, which can be directly compared to the model output.

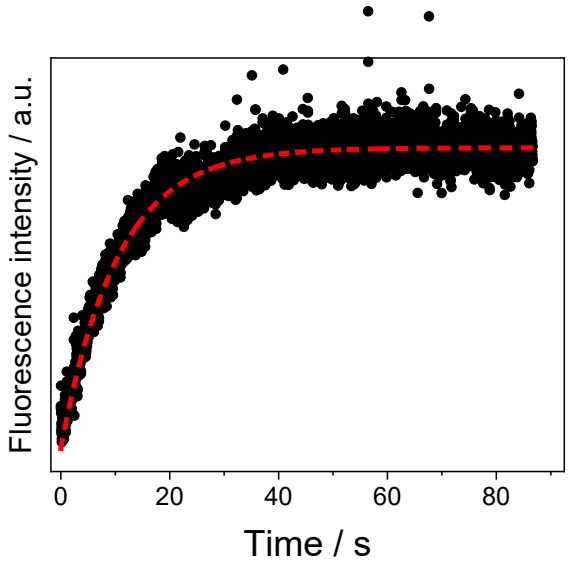

Figure 4: Fluorescence intensity vs. time. The red dashed line indicates the fit to an exponential function to obtain k_{obs} (s^{-1}) as indicated in the main text.

The kinetic data is analyzed using the following assumptions. First, all of the limiting reagent is assumed to be converted to product (i.e., the product formation is irreversible and not treated as

an equilibrium). Second, $Product_1$, $Product_2$, $Product_3$ and $Product_4$ in Fig. 2 have the same quantum yield and these isoindole containing products are the only fluorescent species produced in the reaction. The latter assumption is supported by data reported by Roth,[5] who observed that the fluorescence from an OPA/alanine mixture is comparable to that of a solution containing only OPA. The weak fluorescence from these solutions accounts for only ~0.2% of total signal measured during the reaction of OPA with alanine and mercaptoethanol at pH 9.

A series of kinetic measurements were conducted as a function of pH (7.3-12.6), for solutions with [OPA] = 2.5 mM and [DTT] = [alanine] = 5 mM. Additional kinetics were measured for solutions at a pH = 9, at [OPA] = 0.5, 1.5, and 2.5 mM. In this second set of experiments, [DTT] was fixed at twice the [OPA], and the molar concentration of alanine is always in excess and varied to obtain [alanine]/[OPA] ratios of 1.25, 1.5, 2, 3, 4 and 5.

3.2 Absorbance measurements of OPA solutions

The strong absorbance of OPA between 270-350 nm can be used to estimate the equilibria it establishes with both water and the thiol (Section 3.3). OPA absorbs more strongly when it is "free" (*i.e.* not bound) and its absorbances decreases when hydrated or complexed with DTT.[22] This is used to determine the fraction of bound OPA, enabling an estimate of the equilibrium constants for hydration and its reaction with DTT (*i.e.,* DTT^- and DTT^{2-}).

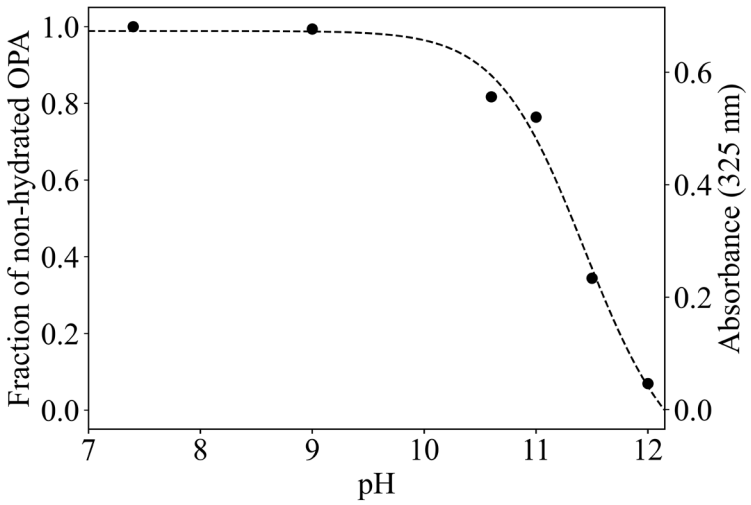

Figure 5: Measured absorbance of 5 mM OPA solutions with variable pH at 325 nm, and corresponding fraction of non-hydrated OPA, calculated assuming that there no hydrated OPA at pH 7.4.

The pH-dependent hydration equilibrium constant of OPA is obtained from absorbance measurements (Ocean Optics Maya2000 PRO) at 325 nm of 5 mM OPA solutions in a 50 mM borate buffer with 4.6 M NaCl. As noted by Salem *et al.*,[22] determining hydration equilibrium coefficients using UV-Vis absorbance can be a challenge due to the overlapping spectra bands of the non-hydrated and hydrated forms of OPA. Using multiple wavelengths, NMR and polarography, Salem *et al.*,[22] showed that assuming only the non-hydrated form of OPA absorbs in the 300 nm region (as we do here), leads, at some temperatures and pH, to an underestimate of the equilibrium constant by up to ~2-4x. Furthermore, Salem *et al.*,[22] showed that the hydration equilibrium constant also depends on ionic strength and water activity. While the conditions used in our study (high ionic strength and a larger pH range) are quite different than those investigated by Salem *et al.*[22], we cannot entirely rule out a similar uncertainty in our spectroscopically determined values of the hydration equilibria of OPA. Since these hydration equilibria are dynamically shifting during the reaction as non-hydrated OPA is consumed to form isoindole, we

don't expect this level of uncertainty to change any of the major conclusions in this study. This is because what is most important for the overall mechanism is the relative rate that these equilibria respond during the reaction, which is we would argue is accurately captured by our measurements. Additionally, our goal is to evaluate the differences between the Sternson-Wong and Simons-Johnson mechanisms, which both assume that non-hydrated OPA is required for the eventual formation of the isoindole product as shown in Fig. 1A and B.

Shown in Fig. 5 is the measured absorbance, which is observed to decrease with increasing pH, indicating a corresponding decrease in the quantity of non-hydrated OPA (Figure 3A) and an increasing amount of hydrated OPA (Figures 3B and C). The overall behavior of the absorbance vs. pH shown in Fig. 5 is consistent with that observed by Salem *et al.*[22] The fraction of non-hydrated OPA (left y-axis in Figure 5) can be calculated assuming that the only absorbing species in solution is non-hydrated OPA and that no hydrated forms are present at pH=7.4, which is consistent with the small difference in absorbance between pH 7.4 and 9 (see Table S2). This assumption is further supported by the measurements by Jacobs *et al.*,[4] who observed only the non-hydrated form of OPA (Fig. 3A) in a mass spectra recorded from an OPA/DTT solution at similarly high ionic strength and at pH 9. Notably, at pH 12 almost all the OPA in solution is hydrated, which has consequences for the quantity of "free" OPA that can ultimately participate in the reaction with DTT and alanine, as discussed in Section 4. As discussed in Section 2, we do not explicitly distinguish between the hydrated forms of OPA, but rather they are lumped together in Table S1 as $OPA_{hydrated}$. From these absorbance measurements we compute the pH-dependent OPA hydration equilibrium constant, used to constrain step 2 in Fig. 2 and in Table S1:

$$K_{hydro} = \frac{[OPA_{hydrated}]}{[OPA]} \quad (3)$$

3.3 Measurements of the pH-dependent OPA-DTT equilibrium

The equilibrium constant for the reaction of OPA and DTT ($K_{eq(OPA\text{-}DTT)}$) is measured as a function of pH, using an approach similar to that used by Trepman *et al.*[12] The absorbance is measured for a series of solutions at a fixed [OPA] (2.5 mM) and a variable concentration of DTT (10^{-5}-10^{-1} M). The decrease in optical density due to the addition of DTT can be directly related to the formation of the OPA-DTT adduct, with the assumption that product absorbance is negligible. However, unlike Trepman's study,[12] we recognize that the hydration of OPA also results in a decrease of the solution absorbance, as described above. Therefore, it is necessary to simultaneously consider these two coupled equilibria to properly model these absorbance measurements and extract $K_{eq(OPA\text{-}DTT)}$. Absorbance spectra for solutions of OPA and DTT at pH 7.4 are shown in Fig. 6. To calculate $K_{eq(OPA\text{-}DTT)}$ we used data at 325 nm (dashed line in Fig. 6), because the absorbance of DTT is negligible at this wavelength but that of OPA is still significant.

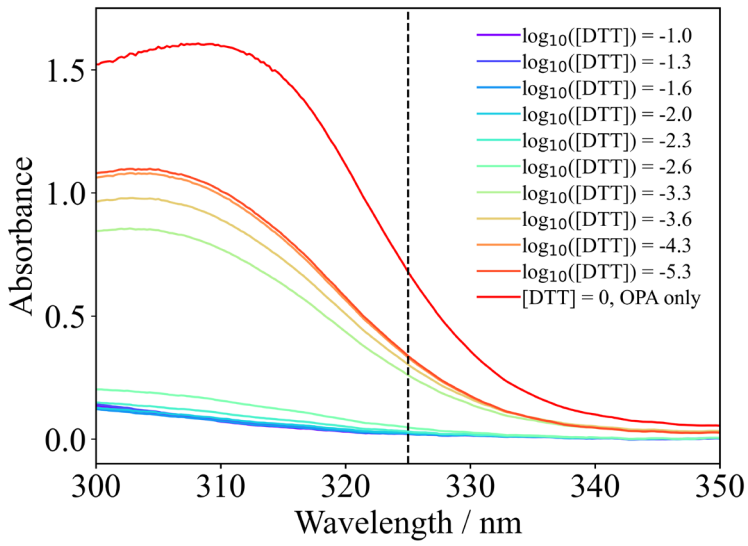

Figure 6: Absorbance of solutions containing OPA (2.5 mM) and DTT (see legend for concentration) at pH 7.4.

Developing a simple analytical expression for the fraction of bound OPA, as was done by Trepman *et al.*,[12] for the two coupled OPA-DTT and OPA hydration equilibria is not possible. Instead, we used a partial model composed of steps 2 and 5 in Table S1 to calculate the concentration of each species at equilibrium. For this determination we neglect DTT speciation (e.g. steps 3 and 4, Table S1). The equilibrium constant for the hydration of OPA (K_{hydro}) is fixed for each pH and as described in Section 3.2. Only OPA reacts with DTT, whereas $OPA_{hydrated}$ is assumed to be non-reactive. DTT has two thiol groups that can both react with OPA, and therefore we include the formation of the OPA-DTT-OPA complex, which is detected by mass spectrometry by Jacobs *et al.*[4] We assume that the equilibrium constants for the formation of OPA-DTT and OPA-DTT-OPA are the same.

The fraction of bound OPA ($\tilde{\nu}$) is computed as the sum of $OPA_{hydrated}$, OPA-DTT and OPA-DTT-OPA at equilibrium. $K_{eq(OPA\text{-}DTT)}$ is floated and the best fit value is determined corresponding to the minimum residual sum of squares (RSS) between the measured and modelled $\tilde{\nu}$ for each dataset at different pH values. Experimental data and best fit curves are shown in Fig. 7A, whereas the pH-dependent best fit values of $K_{eq(OPA\text{-}DTT)}$ are shown in Figure S2. For comparison, Trepman *et al*[12] reported an equilibrium constant for the OPA-metcaptoethanol complex of 165 M^{-1} at pH = 9. Wong *et al.*[2] reported an equilibrium constant for the OPA-mercaptoethanol and OPA-3-mercaptopropionic acid complexes of 215 +/- 25 M^{-1} and 633 +/- 160 M^{-1} at pH = 9.3. Here we find $K_{eq(OPA\text{-}DTT)}$ = 500 M^{-1} at pH =9 (see Figure S2), which is in reasonable agreement with these prior studies given the structural differences between the three thiols. Figure 7B and C show the contributions of $OPA_{hydrated}$, OPA-DTT + OPA-DTT-OPA to the calculated $\tilde{\nu}$. $OPA_{hydrated}$ dominates at low DTT concentrations at high pH, whereas its contribution

to $\tilde{v}$ is small at both low pH where the hydration of OPA is negligible and at high DTT concentrations where the formation of OPA-DTT and OPA-DTT-OPA is favored.

Similar to the observations reported by Trepman *et al.*,[12] we note a small deviation between model and measurements at high concentrations of DTT. They attribute this to the possible formation of a 1:2 OPA-thiol adduct, perhaps resulting from the addition of a thiol group to each of the OPA aldehyde groups. Considering that this deviation is minor, and that the kinetic measurements in Section 3.1 are carried out a much lower concentration of DTT, we have not included this pathway in our model. Finally, it is worth noting that due to the coupled nature of the OPA hydration and OPA-DTT equilibria, the value for $K_{eq(OPA\text{-}DTT)}$ necessarily carries the uncertainty of the measured K_{hydr}.

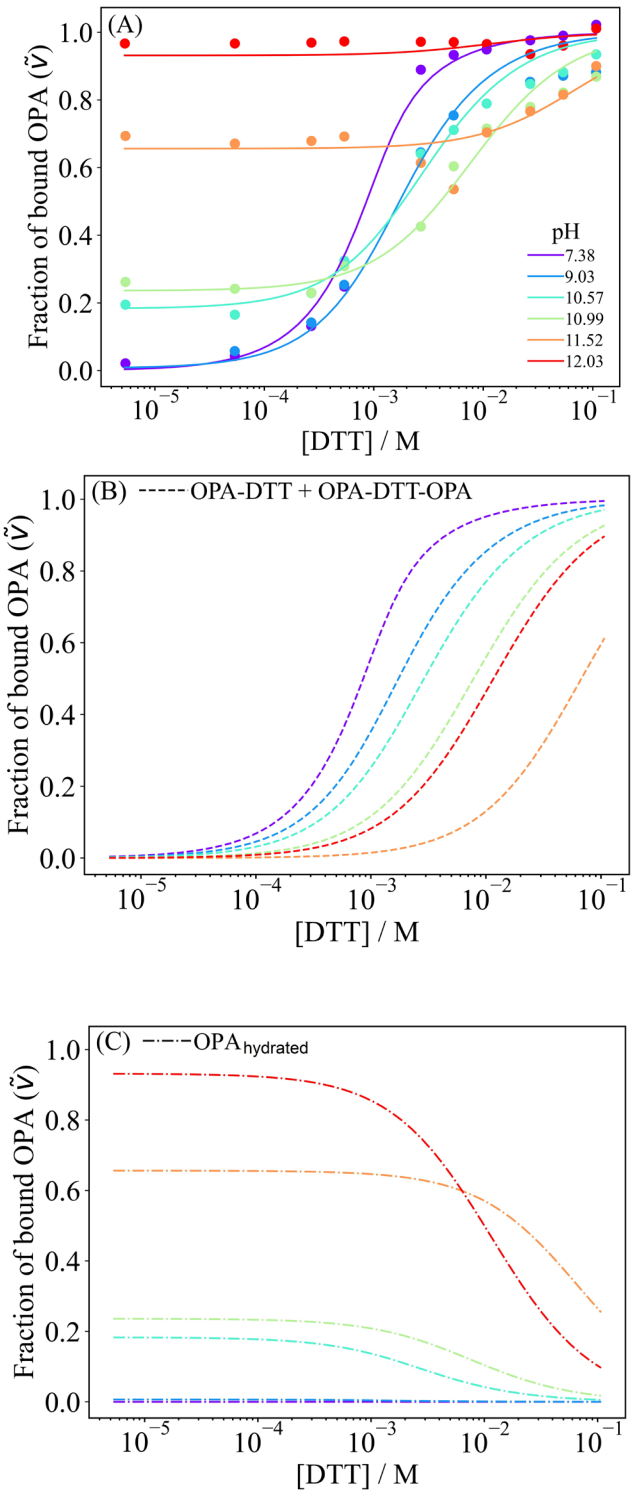

Figure 7: (A) Measured and modelled fraction of bound OPA ($\tilde{v}$) as a function of DTT concentration. $\tilde{v}$ is the sum of $OPA_{hydrated}$, OPA-DTT and OPA-DTT-OPA. (B) Contribution of OPA-DTT and OPA-DTT-OPA to the fraction of bound OPA. (C) Contribution of $OPA_{hydrated}$, to the fraction of bound OPA.

4. Results and Discussion

The best fit of our pH-dependent kinetic measurements of the OPA-alanine-DTT reaction, using the model shown in Table S1 and Fig. 2 is shown in Figure 8. Error bars on the experimental data indicate the standard deviation obtained from an average of 5 repeated measurements. The large error bars for datapoints at pH 10.5-12 arise from the fast kinetics (half time of ~0.25-0.3 s) relative to our mixing times in the cuvette. Therefore, these measurements of k_{obs} are more sensitive to mixing protocols compared to the data obtained at lower or higher pH. Overall, our simulations can reasonably account for the pH-dependence of the reaction using best fit model parameters of k_{i_b} = 0.057 s^{-1}, k_{i_f} = 4.0·10^3 M^{-1} s^{-1} and k_{prod} = 1.1·10^3 M^{-1} s^{-1}. The grey envelope on the model simulation in Figure 8 corresponds to an uncertainty of ± 20% on k_{prod}.

The development of a full kinetic model for this reaction provides significant insights into the factors that govern the overall reaction rate. Our results suggest that the observed pH-dependent kinetics is controlled by the availability of the various species, which participate in the reaction. This is due the coupling of the product formation reaction with several coupled and competing equilibria described in Section 2. One example is the initial concentrations of $Alanine^-$ and OPA at the beginning of the reaction as a function of pH as shown in the Figure S3. The rise in the reaction rate from pH 7 to pH 11 is attributed to the increasing concentration of both $Alanine^-$ and OPA, which results from smaller amounts of OPA-DTT and OPA-DTT-OPA that are formed. The available concentration of non-hydrated and free OPA decreases for pH > ~11 (see Figure S3) due to increasing hydration, resulting in a slowing of the reaction rate in this pH region.

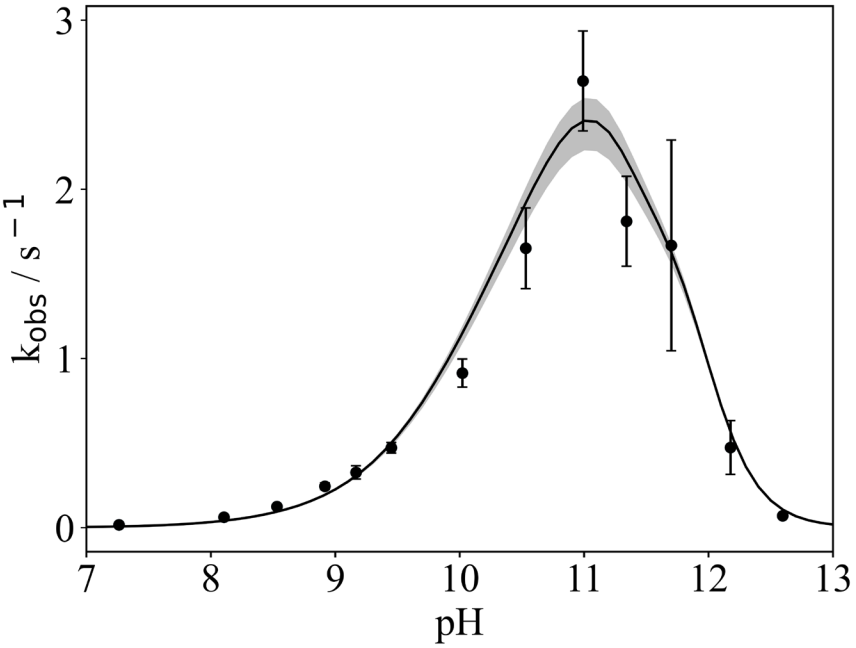

Figure 8: Kinetics measurements (circles) for the reaction between OPA (2.5 mM), DTT (5 mM) and alanine (5 mM) as a function of pH and best fit (solid line) obtained with the model in Table 1. The grey envelope on the model fit corresponds to an uncertainty of ± 20 % on k_{prod}.

Figure S4A compares the fit of the model using the Simons-Johnson mechanism to our pH-dependent data. The results from our simulations using this model are poor for pH > 10, where k_{obs} is largely underestimated compared to measurements. The reason for this is that the Simons-Johnson mechanism involves the reaction of the OPA-thiol complex with the primary amine, but with increasing pH the availability of OPA-DTT (and OPA-DTT-OPA in our case) dramatically decreases as shown in Figure 7B. Therefore, in the Simons-Johnson mechanism the reaction rate is limited by the concentration of OPA-DTT, which results in a significant underestimate of the reaction rate observed in Figure S4A. These results indicate that while the Simons-Johnson mechanism is able to replicate a portion of the pH dependence of k_{obs}, it is not able to capture the full pH range with the same fidelity as the Sternson-Wong mechanism shown in Figure 8.

The model is then tested against our concentration-dependent kinetic measurements at pH 9

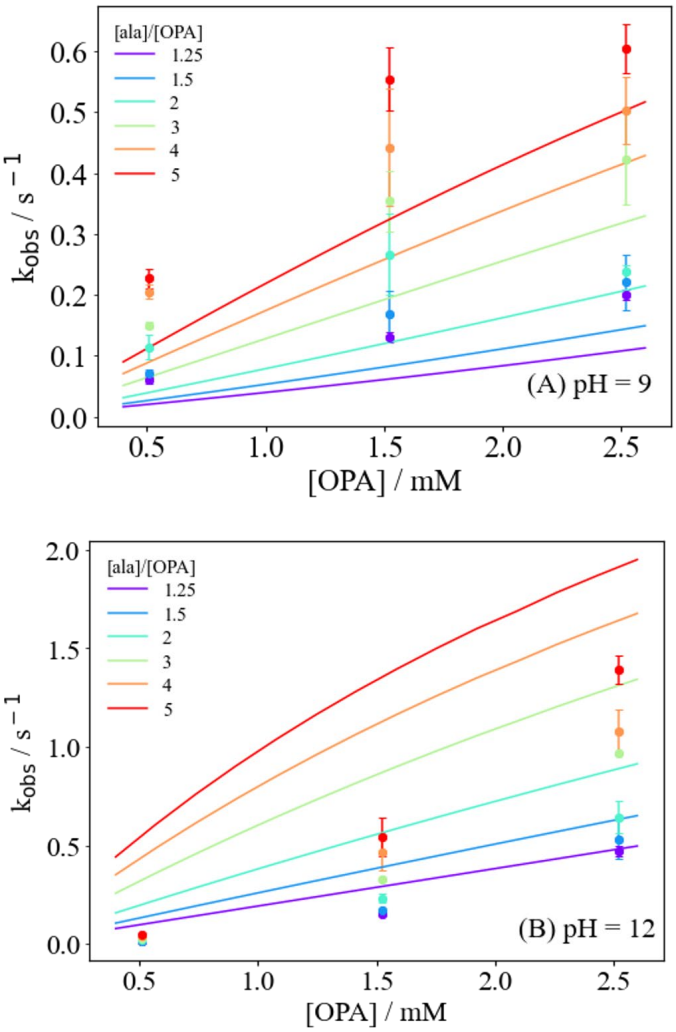

Figure 9: Prediction of k_{obs} (solid lines) for the OPA-alanine-DTT reaction at pH 9 (A) and 12 (B) as a function of alanine/OPA ratio, compared to measurements (solid circles). [OPA] and [DTT] are constant and are 2.5 mM and 5 mM, respectively. Note that solid lines are not a fit but predictions using the best fit parameters obtained from the fitting of the data in Figure 8.

and 12, the results of which are shown in Figure 9 A and B, respectively. Solid circles are k_{obs} from measurements where [DTT] = 2·[OPA], and the concentration of alanine is varied according to the [alanine]/[OPA] ratio shown in the legend of Figure 9. For these measurements alanine is always in excess. The lines are *not* fits of these datasets, but rather predictions resulting from the

best fit model obtained in Figure 8. Overall, the agreement between measurements and model is reasonable, with the model capturing the overall trends in the pH 9 and 12 data to within a factor of 2 or less. This is in contrast to the Simons-Johnson mechanism shown in Fig. S4 where, as expected, the pH 9 experimental results are reasonably well-reproduced, but at pH 12 there is substantial deviation from the experimental data.

Further evaluation of our kinetic model was performed by simulating the reaction kinetics measured by Trepman *et al.*[12] and Wong *et al*.[2] Trepman *et al.*[12] measured the pH-dependent kinetics of the reaction between OPA, alanine and mercaptoethanol (ME). Considering the differences in structure between DTT (2 SH groups) and mercaptoethanol (1 SH group), we introduced the following modifications in order to simulate their measurements. First, we removed Steps 4, 5b, 5c, 5d, 8, 9 and 10 in Table S1, since these steps require two thiol groups. Finally, we took the value of $K_{eq(OPA\text{-}ME)}$ (215 M^{-1}) at pH = 9.3 from Wong *et al.*[2] and used it to rescale our measured pH-dependence of $K_{eq(OPA\text{-}DTT)}$ shown in Figure S2. All other parameters in the model are left unchanged from the best fit model in Figure 8.

Figure S5A shows the comparison between measurements from Trepman *et al.*[12] conducted at [OPA] = 1 mM, [ME] = 2.86 mM, [alanine] = 10^{-2} mM (Figure 5 in their publication) and our model simulations. The pseudo-first order rate constant k_0 is calculated in Trepman *et al*.[12] as $k_0 = 0.693/t_{1/2}$, where $t_{1/2}$ is the time of half reaction. Our prediction correctly reproduces the pH-dependent shape of k_0 but overestimates their data by ~50% at pH between 10 and 11.5. This difference is likely due to the dithiol used in the development of our model compared with the monothiol (ME) used by Trepman *et al.* In fact, if we run a prediction with $k_{prod} \cdot 0.5$ to account for the presence of only one SH group the model/experimental agreement is substantially improved.

Both Wong *et al.*[2] (Figure 1 in their work) and Trepman *et al.*[12] (Figure 6A in their work) measured the kinetics of the reaction between OPA and alanine as a function of mercaptoethanol concentration at pH ~ 9.3. Figure S5B and C shows that our model is able to capture the order of magnitude of the measured rate constants but is unable to fully reproduce the trend of their thiol concentration-dependent data. The reason for this discrepancy is currently unclear but may suggest that the high ionic strength used in our experiments is either accelerating or decelerating certain reaction steps relative to the experimental conditions used by Wong *et al.*[2] and Trepman *et al.*[12]

In summary, we conclude that our overall kinetic framework is qualitatively robust, and that the Sternson-Wong mechanism provides the best description of both our new kinetic measurements and prior literature measurements of the OPA-alanine-thiol reaction kinetics as a function of: (1) pH (quantitatively), (2) OPA concentration (quantitatively) and (3) thiol concentration (qualitatively).

5. Conclusions

In this work, we present measurements and kinetic modelling of the reaction of OPA, alanine and DTT (a dithiol). We used pH-dependent measured reaction rates to evaluate two different reaction mechanism proposed in the literature, one where OPA and alanine react first and the thiol is added in the last step (Sternson-Wong mechanism), and the other where alanine is added last to an OPA-thiol complex (Simons-Johnson mechanism). We found that the Sternson-Wong mechanism best describes our pH-dependent measurements and best predicts the concentration-dependent kinetics measured at pH 9 and 12. The model based on the Simons-Johnson mechanism is not able to reproduce our experimental results at high pH, where it significantly underestimates

the reaction rates. We suggest the reason for this is the decreasing amount of available OPA-DTT (and OPA-DTT-OPA) with increasing pH, which limits the overall reaction rate.

The kinetic studies in this work contribute to the literature discussion on the reaction mechanism between OPA, primary amines and thiols. This reaction is widely used in analytical applications for the quantification of primary amines, for example in peptides and proteins. Improved knowledge of the reaction mechanism can lead to the optimization of these analytical approaches and to the design of improved OPA derivatives. Furthermore, the OPA-alanine-DTT reaction rates were observed to be accelerated in aqueous microdroplets and the kinetic model developed in this work will be used to provide deeper insight into possible in-droplet acceleration mechanism(s).

Supplementary Information: Additional reaction schemes, Figures and Tables including details on the reaction mechanisms, rate and equilibrium constants, and kinetic measurements.

Acknowledgements: This work was supported by the Condensed Phase and Interfacial Molecular Science Program (CPIMS), in the Chemical Sciences Geosciences and Biosciences Division of the Office of Basic Energy Sciences of the U.S. Department of Energy under Contract No. DE-AC02-05CH11231.

References

1. L. A. Sternson, J. F. Stobaugh and A. J. Repta, Rational design and evaluation of improved o-phthalaldehyde-like fluorogenic reagents, *Anal. Biochem.*, 1985, **144**, 233-246.

2. O. S. Wong, L. A. Sternson and R. L. Schowen, Reaction of o-phthalaldehyde with alanine and thiols: kinetics and mechanism, *J. Am. Chem. Soc.*, 1985, **107**, 6421-6422.

3. S. S. Simons, Jr. and D. F. Johnson, Reaction of o-phthalaldehyde and thiols with primary amines: formation of 1-alkyl(and aryl)thio-2-alkylisoindoles, *J. Org. Chem.*, 1978, **43**, 2886-2891.

4. M. I. Jacobs, J. F. Davies, L. Lee, R. D. Davis, F. Houle and K. R. Wilson, Exploring Chemistry in Microcompartments Using Guided Droplet Collisions in a Branched Quadrupole Trap Coupled to a Single Droplet, Paper Spray Mass Spectrometer, *Anal. Chem.*, 2017, **89**, 12511-12519.

5. M. Roth, Fluorescence reaction for amino acids, *Anal. Chem.*, 1971, **43**, 880-882.

6. J. R. Benson and P. Hare, O-phthalaldehyde: fluorogenic detection of primary amines in the picomole range. Comparison with fluorescamine and ninhydrin, *Proc. Natl. Acad. Sci. U.S.A.*, 1975, **72**, 619-622.

7. P. Zuman, Reactions of Orthophthalaldehyde with Nucleophiles, *Chem. Rev.*, 2004, **104**, 3217-3238.

8. J. Cronin and P. Hare, Chromatographic analysis of amino acids and primary amines with o-phthalaldehyde detection, *Anal. Biochem.*, 1977, **81**, 151-156.

9. W. J. M. Underberg and J. C. M. Waterval, Derivatization trends in capillary electrophoresis: An update, *Electrophoresis*, 2002, **23**, 3922-3933.

10. S. S. Simons, Jr. and D. F. Johnson, The structure of the fluorescent adduct formed in the reaction of o-phthalaldehyde and thiols with amines, *J. Am. Chem. Soc.*, 1976, **98**, 7098-7099.

11. P. Zuman, N. Salem and E. Kulla, What Do We Know about Determination of Amino Acids with Orthophthalaldehyde?, *Electroanalysis*, 2009, **21**, 645-649.

12. E. Trepman and R. F. Chen, Fluorescence stopped-flow study of the o-phthaldialdehyde reaction, *Arch. Biochem. Biophys.*, 1980, **204**, 524-532.

13. J. D. Dazie, A. Liška and J. Ludvík, Electrochemical and Quantum Chemical Study of Reactivity of Orthophthalaldehyde with Aliphatic Primary Amines, *J. Electrochem. Soc.*, 2016, **163**, G127.

14. Z. Wei, Y. Li, R. G. Cooks and X. Yan, Accelerated Reaction Kinetics in Microdroplets: Overview and Recent Developments, *Ann. Rev. Phys. Chem.*, 2020, **71**, 31-51.

15. A. Fallah-Araghi, K. Meguellati, J.-C. Baret, A. E. Harrak, T. Mangeat, M. Karplus, S. Ladame, C. M. Marques and A. D. Griffiths, Enhanced Chemical Synthesis at Soft Interfaces: A Universal Reaction-Adsorption Mechanism in Microcompartments, *Phys. Rev. Lett.*, 2014, **112**, 028301.

16. K. R. Wilson, A. M. Prophet, G. Rovelli, M. D. Willis, R. J. Rapf and M. I. Jacobs, A kinetic description of how interfaces accelerate reactions in micro-compartments, *Chem. Sci.*, 2020, **11**, 8533-8545.

17. C. F. Chamberlayne and R. N. Zare, Simple model for the electric field and spatial distribution of ions in a microdroplet, *J. Chem. Phys.*, 2020, **152**, 184702.

18. C. F. Chamberlayne and R. N. Zare, Microdroplets can act as electrochemical cells, *J. Chem. Phys.*, 2022, **156**, 054705.

19. G. Rovelli, M. I. Jacobs, M. D. Willis, R. J. Rapf, A. M. Prophet and K. R. Wilson, A critical analysis of electrospray techniques for the determination of accelerated rates and mechanisms of chemical reactions in droplets, *Chem. Sci.*, 2020, **11**, 13026-13043.

20. M. C. García Alvarez-Coque, M. J. M. Hernández, R. M. Villanueva Camañas and C. Mongay Fernández, Studies on the formation and stability of isoindoles derived from amino acids, o-phthalaldehyde and N-acetyl-l-cysteine, *Anal. Biochem.*, 1989, **180**, 172-176.

21. M. Eigen, Proton Transfer, Acid-Base Catalysis, and Enzymatic Hydrolysis. Part I: Elementary Processes, *Angew. Chem.*, 1964, **3**, 1-19.

22. N. Salem, S. Andreescu, E. Kulla and P. Zuman, Existence and Reactivity of Three Forms of Orthophthalaldehyde in Aqueous Solutions. Polarographic, Voltammetric, and Spectrophotometric Study, *J. Phys. Chem. A*, 2007, **111**, 4658-4670.

23. O. S. Wong, L. A. Sternson and R. L. Schowen, Correction. Reaction of o-Phthalaldehyde with Alanine and Thiols: Kinetics and Mechanism, *J. Am. Chem. Soc.*, 1986, **108**, 1361-1361.

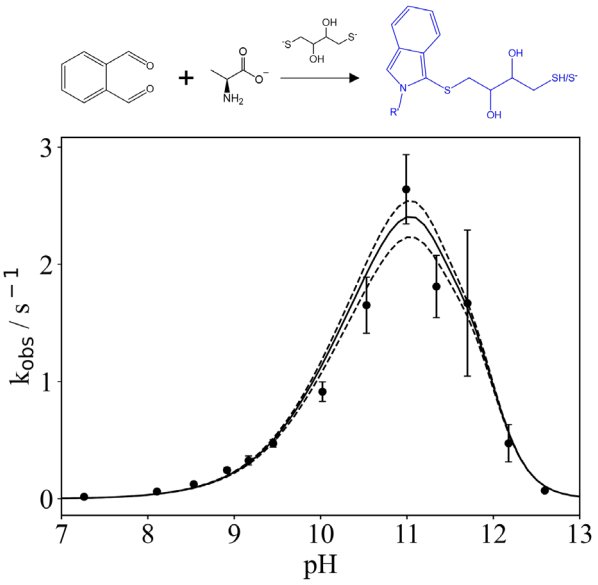

TOC Graphic

Supplementary Information for:

Elucidating the Mechanism for the Reaction of o-phthalaldehyde with Primary Amines in the Presence of Thiols

Grazia Rovelli,[a] and Kevin R. Wilson [a]

[a] Chemical Sciences Division, Lawrence Berkeley National Laboratory, Berkeley, 94720, CA, USA

Contents:

S1. Reaction scheme and ODE model: Sternson-Wong mechanism

$$OPA \underset{k_{hydro_b}}{\overset{k_{hydro_f}}{\rightleftharpoons}} OPA_{hydrated}$$

$$DTT \underset{k_{DTT_b}}{\overset{k_{DTT_f}}{\rightleftharpoons}} DTT^{-}$$

$$DTT^{-} \underset{k_{DTT_b}}{\overset{k_{DTT_f}}{\rightleftharpoons}} DTT^{2-}$$

$$DTT^{-} + OPA \underset{k_{OPA\text{-}DTT_b}}{\overset{k_{OPA\text{-}DTT_f}}{\rightleftharpoons}} OPA\text{-}DTT_1$$

$$DTT^{2-} + OPA \underset{k_{OPA\text{-}DTT_b}}{\overset{k_{OPA\text{-}DTT_f}}{\rightleftharpoons}} OPA\text{-}DTT_2{}^{-}$$

$$OPA\text{-}DTT_2{}^{-} + OPA \underset{k_{OPA\text{-}DTT_b}}{\overset{k_{OPA\text{-}DTT_f}}{\rightleftharpoons}} OPA\text{-}DTT\text{-}OPA$$

$$Alanine \underset{k_{ala_b}}{\overset{k_{ala_f}}{\rightleftharpoons}} Alanine^{-}$$

$$OPA + Alanine^{-} \underset{k_{i_b}}{\overset{k_{i_f}}{\rightleftharpoons}} I$$

$$I + DTT^{-} \xrightarrow{k_{prod}} Product_1$$

$$I + DTT^{2-} \xrightarrow{k_{prod}} Product_2{}^{-}$$

$$I + Product_2{}^{-} \xrightarrow{k_{prod}} Product_3$$

$$Product_2{}^{-} + OPA \underset{k_{OPA\text{-}DTT_b}}{\overset{k_{OPA\text{-}DTT_f}}{\rightleftharpoons}} Product_4$$

$$OPA\text{-}DTT_2{}^{-} + I \xrightarrow{k_{prod}} Product_4$$

$$\frac{d[OPA]}{dt} = -k_{hydro_f}[OPA] + k_{hydro_b}[OPA_{hydrated}] - k_{OPA\text{-}DTT_f}[OPA][DTT^-] + k_{OPA\text{-}DTT_b}[OPA\text{-}DTT_1]$$
$$-k_{OPA\text{-}DTT_f}[OPA][DTT^{2-}] + k_{OPA\text{-}DTT_b}[OPA\text{-}DTT_2{}^-]$$
$$-k_{OPA\text{-}DTT_f}[OPA][OPA\text{-}DTT_2{}^-] + k_{OPA\text{-}DTT_b}[OPA\text{-}DTT\text{-}OPA]$$
$$-k_{i,f}[OPA][Alanine^-] + k_{i,b}[I]$$
$$-k_{OPA\text{-}DTT_f}[OPA][Product_2{}^-] + k_{OPA\text{-}DTT_b}[Product_4]$$

$$\frac{d[OPA_{hydrated}]}{dt} = +k_{hydro_f}[OPA] - k_{hydro_b}[OPA_{hydrated}]$$

$$\frac{d[DTT]}{dt} = -k_{DTT_f}[DTT] + k_{DTT_b}[DTT^-]$$

$$\frac{d[DTT^-]}{dt} = +k_{DTT_f}[DTT] - k_{DTT_b}[DTT^-] - k_{DTT_f}[DTT^-] + k_{DTT_b}[DTT^{2-}]$$
$$-k_{OPA\text{-}DTT_f}[OPA][DTT^-] + k_{OPA\text{-}DTT_b}[OPA\text{-}DTT_1] - k_{prod}[I][DTT^-]$$

$$\frac{d[DTT^{2-}]}{dt} = +k_{DTT_f}[DTT^-] - k_{DTT_b}[DTT^{2-}]$$
$$-k_{OPA\text{-}DTT_f}[OPA][DTT^{2-}] + k_{OPA\text{-}DTT_b}[OPA\text{-}DTT_2{}^-] - k_{prod}[I][DTT^{2-}]$$

$$\frac{d[OPA\text{-}DTT_1]}{dt} = +k_{OPA\text{-}DTT_f}[OPA][DTT^-] - k_{OPA\text{-}DTT_b}[OPA\text{-}DTT_1]$$

$$\frac{d[OPA\text{-}DTT_2{}^-]}{dt} = +k_{OPA\text{-}DTT_f}[OPA][DTT^{2-}] - k_{OPA\text{-}DTT_b}[OPA\text{-}DTT_2{}^-] - k_{OPA\text{-}DTT_f}[OPA][OPA\text{-}DTT_2{}^-]$$
$$+k_{OPA\text{-}DTT_b}[OPA\text{-}DTT\text{-}OPA] - k_{prod}[OPA\text{-}DTT_2{}^-][I]$$

$$\frac{d[OPA\text{-}DTT\text{-}OPA]}{dt} = +k_{OPA\text{-}DTT_f}[OPA][OPA\text{-}DTT_2{}^-] - k_{OPA\text{-}DTT_b}[OPA\text{-}DTT\text{-}OPA]$$

$$\frac{d[Alanine]}{dt} = -k_{ala_f}[Alanine] + k_{ala_b}[Alanine^-]$$
$$\frac{d[Alanine^-]}{dt} = +k_{ala_f}[Alanine] - k_{ala_b}[Alanine^-] - k_{i,f}[OPA][Alanine^-] + k_{i,b}[I]$$

$$\frac{d[I]}{dt} = +k_{i,f}[OPA][Alanine^-] - k_{i,b}[I] - k_{prod}[I][DTT^-] - k_{prod}[I][DTT^{2-}]$$
$$-k_{prod}[I][Product_2{}^-] - k_{prod}[I][OPA\text{-}DTT_2]$$

$$\frac{d[Product_1]}{dt} = +k_{prod}[I][DTT^-]$$

$$\frac{d[Product_2{}^-]}{dt} = +k_{prod}[I][DTT^{2-}] - k_{prod}[I][Product_2{}^-]$$
$$-k_{OPA\text{-}DTT_f}[OPA][Product_2{}^-] + k_{OPA\text{-}DTT_b}[Product_4]$$

$$\frac{d[Product_3]}{dt} = +k_{prod}[I][Product_2{}^-]$$

$$\frac{d[Product_4]}{dt} = +k_{prod}[I][OPA\text{-}DTT_2] + k_{OPA\text{-}DTT_f}[OPA][Product_2{}^-] - k_{OPA\text{-}DTT_b}[Product_4]$$

S2. Reaction scheme and ODE model: Simons-Johnson mechanism

$$OPA \underset{k_{hydro_b}}{\overset{k_{hydro_f}}{\rightleftharpoons}} OPA_{hydrated}$$

$$DTT \underset{k_{DTT_b}}{\overset{k_{DTT_f}}{\rightleftharpoons}} DTT^{-}$$

$$DTT^{-} \underset{k_{DTT_b}}{\overset{k_{DTT_f}}{\rightleftharpoons}} DTT^{2-}$$

$$DTT^{-} + OPA \underset{k_{OPA\text{-}DTT_b}}{\overset{k_{OPA\text{-}DTT_f}}{\rightleftharpoons}} OPA\text{-}DTT_1$$

$$DTT^{2-} + OPA \underset{k_{OPA\text{-}DTT_b}}{\overset{k_{OPA\text{-}DTT_f}}{\rightleftharpoons}} OPA\text{-}DTT_2{}^{-}$$

$$OPA\text{-}DTT_2{}^{-} + OPA \underset{k_{OPA\text{-}DTT_b}}{\overset{k_{OPA\text{-}DTT_f}}{\rightleftharpoons}} OPA\text{-}DTT\text{-}OPA$$

$$Alanine \underset{k_{ala_b}}{\overset{k_{ala_f}}{\rightleftharpoons}} Alanine^{-}$$

$$OPA\text{-}DTT_1 + Alanine^{-} \xrightarrow{k_{prod}} Product_1$$

$$OPA\text{-}DTT_2{}^{-} + Alanine^{-} \xrightarrow{k_{prod}} Product_2{}^{-}$$

$$OPA\text{-}DTT\text{-}OPA + Alanine^{-} \xrightarrow{k_{prod}} Product_3$$

$$Product_2{}^{-} + OPA \underset{k_{OPA\text{-}DTT_b}}{\overset{k_{OPA\text{-}DTT_f}}{\rightleftharpoons}} Product_4$$

$$\frac{d[OPA]}{dt} = -k_{hydro_f}[OPA] + k_{hydro_b}[OPA_{hydrated}] - k_{OPA\text{-}DTT_f}[OPA][DTT^-] + k_{OPA\text{-}DTT_b}[OPA\text{-}DTT_1]$$
$$-k_{OPA\text{-}DTT_f}[OPA][DTT^{2-}] + k_{OPA\text{-}DTT_b}[OPA\text{-}DTT_2]$$
$$-k_{OPA\text{-}DTT_f}[OPA][OPA\text{-}DTT_2] + k_{OPA\text{-}DTT_b}[OPA\text{-}DTT\text{-}OPA]$$
$$-k_{OPA\text{-}DTT_f}[OPA]\left[Product_2{}^-\right] + k_{OPA\text{-}DTT_b}[Product_4]$$

$$\frac{d[OPA_{hydrated}]}{dt} = +k_{hydro_f}[OPA] - k_{hydro_b}[OPA_{hydrated}]$$

$$\frac{d[DTT]}{dt} = -k_{DTT_f}[DTT] + k_{DTT_b}[DTT^-]$$

$$\frac{d[DTT^-]}{dt} = +k_{DTT_f}[DTT] - k_{DTT_b}[DTT^-] - k_{DTT_f}[DTT^-] + k_{DTT_b}[DTT^{2-}]$$
$$-k_{OPA\text{-}DTT_f}[OPA][DTT^-] + k_{OPA\text{-}DTT_b}[OPA\text{-}DTT_1]$$

$$\frac{d[DTT^{2-}]}{dt} = +k_{DTT_f}[DTT^-] - k_{DTT_b}[DTT^{2-}]$$
$$-k_{OPA\text{-}DTT_f}[OPA][DTT^{2-}] + k_{OPA\text{-}DTT_b}[OPA\text{-}DTT_2]$$

$$\frac{d[OPA\text{-}DTT_1]}{dt} = +k_{OPA\text{-}DTT_f}[OPA][DTT^-] - k_{OPA\text{-}DTT_b}[OPA\text{-}DTT_1] - k_{prod}[OPA\text{-}DTT_1][Alanine^-]$$

$$\frac{d[OPA\text{-}DTT_2]}{dt} = +k_{OPA\text{-}DTT_f}[OPA][DTT^{2-}] - k_{OPA\text{-}DTT_b}[OPA\text{-}DTT_2] - k_{OPA\text{-}DTT_f}[OPA][OPA\text{-}DTT_2]$$
$$+k_{OPA\text{-}DTT_b}[OPA\text{-}DTT\text{-}OPA] - k_{prod}[OPA\text{-}DTT_2][Alanine^-]$$

$$\frac{d[OPA\text{-}DTT\text{-}OPA]}{dt} = +k_{OPA\text{-}DTT_f}[OPA][OPA\text{-}DTT_2] - k_{OPA\text{-}DTT_b}[OPA\text{-}DTT\text{-}OPA]$$
$$-k_{prod}[OPA\text{-}DTT\text{-}OPA][Alanine^-]$$

$$\frac{d[Alanine]}{dt} = -k_{ala_f}[Alanine] + k_{ala_b}[Alanine^-]$$

$$\frac{d[Alanine^-]}{dt} = +k_{ala_f}[Alanine] - k_{ala_b}[Alanine^-] - k_{prod}[OPA\text{-}DTT_1][Alanine^-]$$
$$-k_{prod}[OPA\text{-}DTT_2][Alanine^-] - k_{prod}[OPA\text{-}DTT\text{-}OPA][Alanine^-]$$

$$\frac{d[Product_1]}{dt} = +k_{prod}[OPA\text{-}DTT_1][Alanine^-]$$

$$\frac{d[Product_2{}^-]}{dt} = +k_{prod}[OPA\text{-}DTT_2][Alanine^-] - k_{OPA\text{-}DTT_f}[OPA]\left[Product_2{}^-\right] + k_{OPA\text{-}DTT_b}[Product_4]$$

$$\frac{d[Product_3]}{dt} = +k_{prod}[OPA\text{-}DTT\text{-}OPA][Alanine^-]$$

$$\frac{d[Product_4]}{dt} = +k_{OPA\text{-}DTT_f}[OPA]\left[Product_2{}^-\right] - k_{OPA\text{-}DTT_b}[Product_4]$$

Figures:

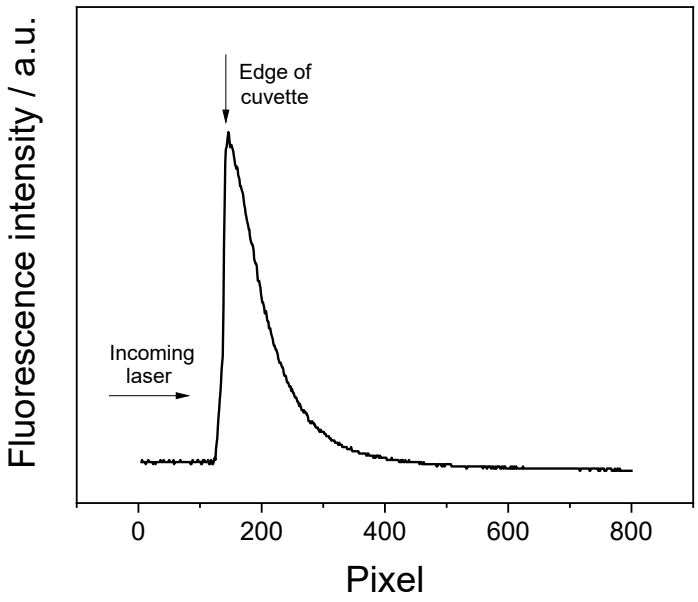

Figure S1: Fluorescence intensity profile arising from the excitation with a 355 nm laser of the isoindole product across the cuvette volume. For clarity, the direction of the incoming laser and the edge of the cuvette are indicated by arrows. The intensity of the fluorescent signal decreases through the volume of the cuvette, indicating that the product is self-absorbing.

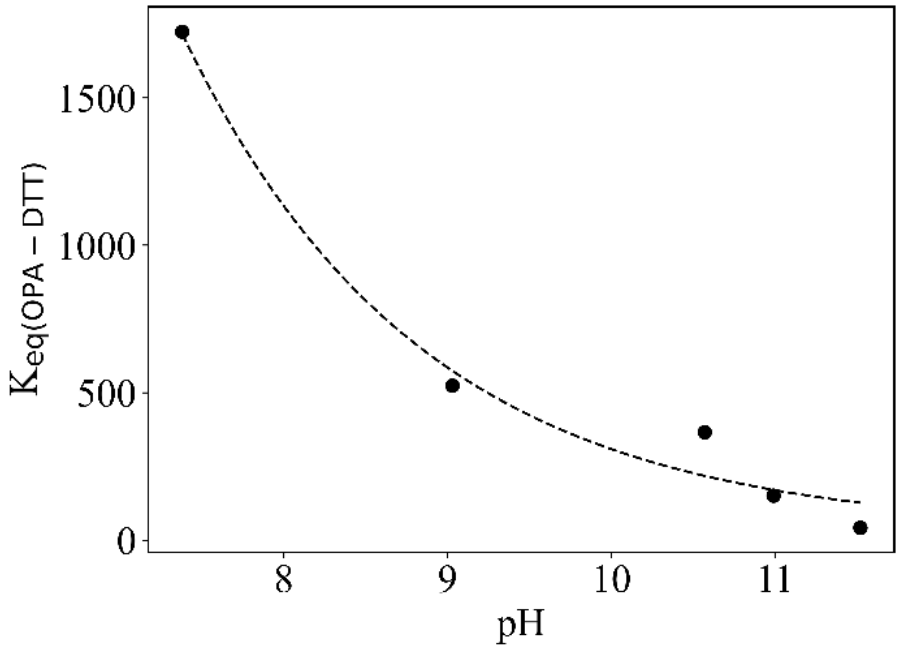

Figure S2: Measured equilibrium constants ($K_{eq(OPA\text{-}DTT)}$, M^{-1}) for the reaction between OPA and DTT and a polynomial fit (dashed line) of experimental data.

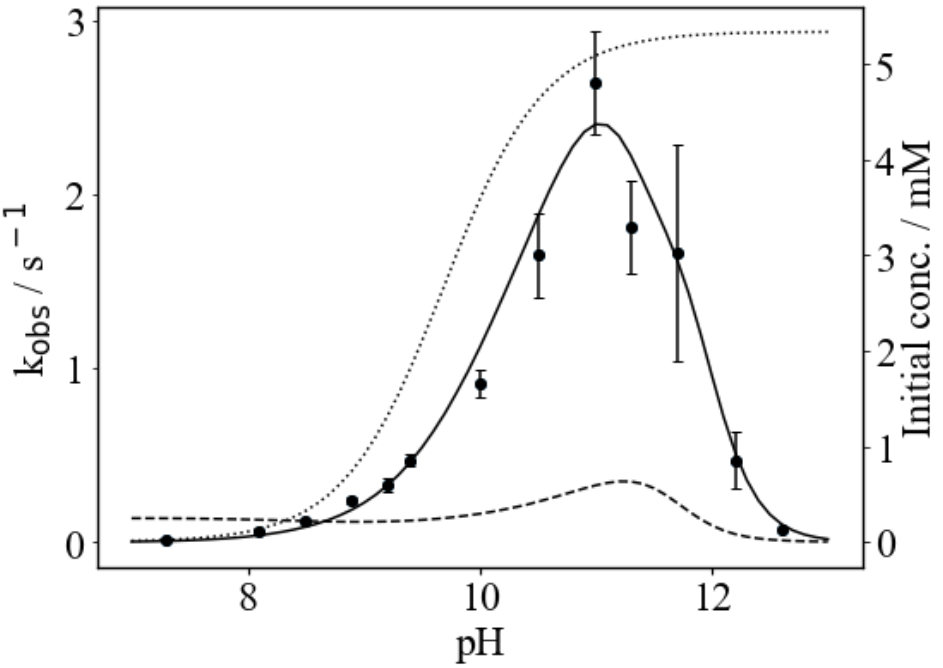

Figure S3: Comparison of the measured and fitted reaction kinetics (left axis) with the initial concentrations (right axis) of OPA (dashed line) and Alanine$^-$ (dotted line).

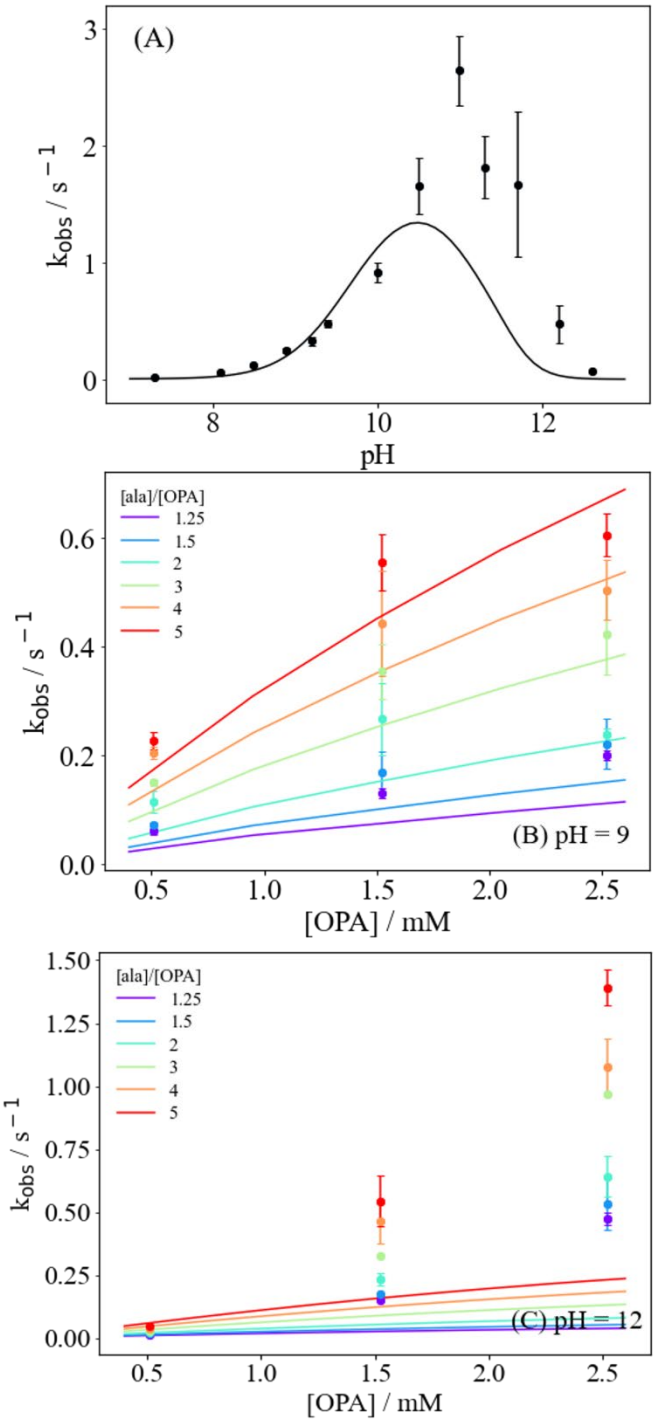

Figure S4: (A) Fitting of the measured pH-dependent kinetics with the Simons-Johnson mechanism. Prediction of reaction rates at pH = 9 (B) and 12 (C) using the model in Panel (A).

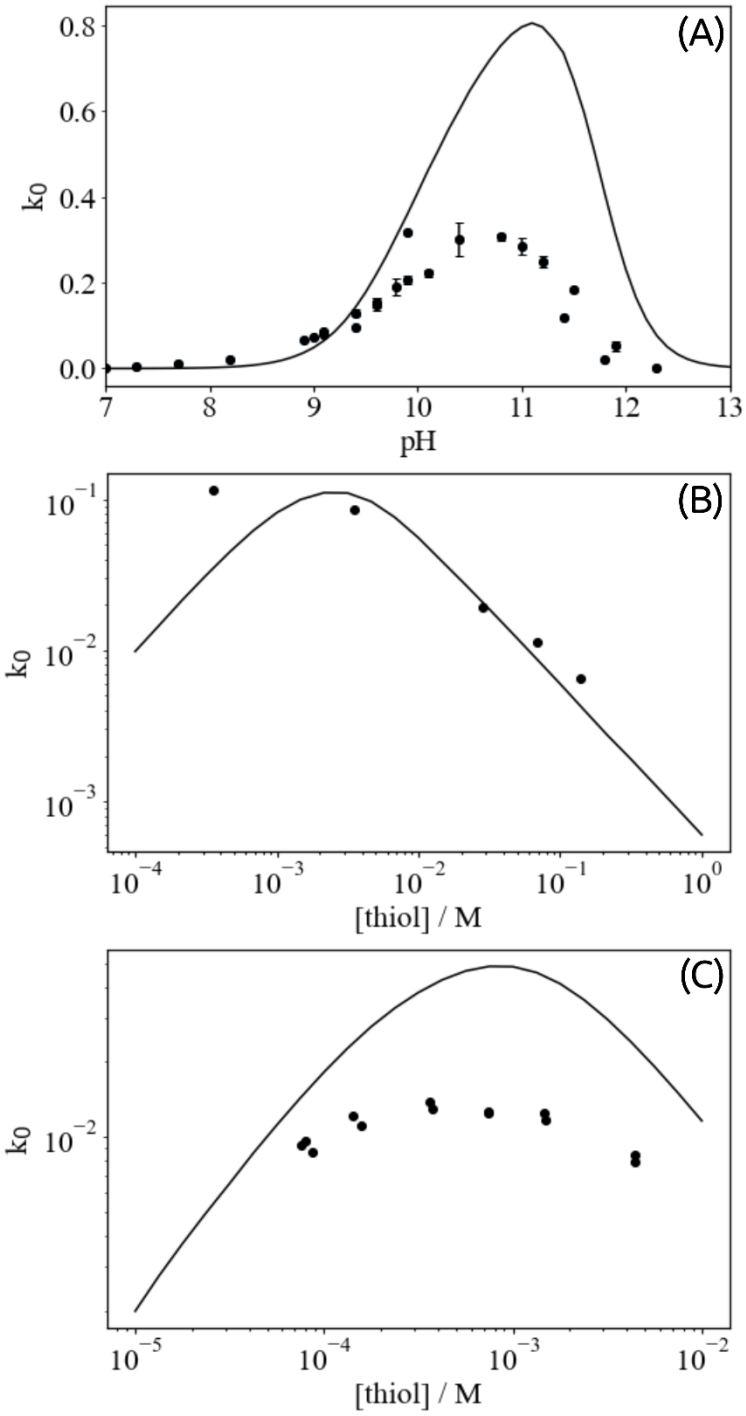

Figure S5: Prediction of pH-dependent rate constants for the OPA-alanine-ME reaction in: (A) the thiol concentration-dependent kinetics of Trepman et al[1]. (B) The thiol concentration-dependent kinetics in Wong et al.[2] (C) for the reaction with ME. All prediction use the best k_{prod} from the fit in Figure 9 (black solid line).

Tables

Table S1: Elementary steps and rate constant based on the Sternson-Wong mechanism. Reaction steps and molecular structures are shown in Figure 2.

Step	Reaction	Constant	Description	Value	Unit
1	$Alanine \underset{k_{ala_b}}{\overset{k_{ala_f}}{\rightleftharpoons}} Alanine^-$	k_{ala_f}	Calculated from alanine's amine deprotonation $pK_a = 9.69$	pH-dependent	s^{-1}
		k_{ala_b}	Assumed to be diffusion limited	10^{10}	s^{-1}
2	$OPA \underset{k_{hydro_b}}{\overset{k_{hydro_f}}{\rightleftharpoons}} OPA_{hydrated}$	k_{hydro_f}	Constrained to the measured K_{hydro} and k_{hydro_b}	pH-dependent	s^{-1}
		k_{hydro_b}	Salem et al.[21]	pH-dependent	s^{-1}
3	$DTT \underset{k_{DTT_b}}{\overset{k_{DTT_f}}{\rightleftharpoons}} DTT^-$	k_{DTT_f}	From DTT first dissociation constant $pK_a = 9.2$	pH-dependent	s^{-1}
		k_{DTT_b}	Assumed to be diffusion limited	10^{10}	s^{-1}
4	$DTT^- \underset{k_{DTT_b}}{\overset{k_{DTT_f}}{\rightleftharpoons}} DTT^{2-}$	k_{DTT_f}	From DTT second dissociation constant $pK_a = 10.1$	pH-dependent	s^{-1}
		k_{DTT_b}	Assumed to be diffusion limited	10^{10}	s^{-1}
5	(a) $OPA + DTT^- \underset{k_{OPA-DTT_b}}{\overset{k_{OPA-DTT_f}}{\rightleftharpoons}} OPA-DTT_1$ (b) $OPA + DTT^{2-} \underset{k_{OPA-DTT_b}}{\overset{k_{OPA-DTT_f}}{\rightleftharpoons}} OPA-DTT_2^-$ (c) $OPA-DTT_2^- + OPA \underset{k_{OPA-DTT_b}}{\overset{k_{OPA-DTT_f}}{\rightleftharpoons}} OPA-DTT-OPA$ (d) $OPA + Product_2{}^- \underset{k_{OPA-DTT_b}}{\overset{k_{OPA-DTT_f}}{\rightleftharpoons}} Product_4$	$k_{OPA\text{-}DTT_f}$	Constrained to the measured $K_{eq(OPA\text{-}DTT)}$ and $k_{OPA\text{-}DTT_b}$	pH-dependent	$M^{-1}\ s^{-1}$
		$k_{OPA\text{-}DTT_b}$	Fit parameter, but constrained to the measured $K_{eq(OPA\text{-}DTT)} = k_{OPA\text{-}DTT_f}/k_{OPA\text{-}DTT_b}$	10^3	s^{-1}
6	$OPA + Alanine^- \underset{k_{i_b}}{\overset{k_{i_f}}{\rightleftharpoons}} I$	k_{i_f}	Fit parameter	$4.0 \cdot 10^3$	$M^{-1}\ s^{-1}$
		k_{i_b}	Fit parameter	0.057	s^{-1}
7	$I + DTT^- \xrightarrow{k_{prod}} Product_1$	k_{prod}	Fit parameter	$1.1 \cdot 10^3$	$M^{-1}\ s^{-1}$
8	$I + DTT^{2-} \xrightarrow{k_{prod}} Product_2{}^-$				
9	$I + OPA-DTT_2^- \xrightarrow{k_{prod}} Product_4$	k_{prod}	Fit parameter	$1.1 \cdot 10^3$	$M^{-1}\ s^{-1}$
10	$I + Product_2{}^- \xrightarrow{k_{prod}} Product_3$	k_{prod}	Fit parameter	$1.1 \cdot 10^3$	$M^{-1}\ s^{-1}$

Table S2: Absorbance measurements of 5 mM solutions at 325 nm as a function of pH, together with the corresponding calculated fraction of non-hydrated OPA and K_{hydr} values.

pH	Absorbance	Fraction of non-hydrated OPA	$\boldsymbol{K_{hydro}}$
7.4	0.683	1.000	0.000
9.0	0.678	0.994	0.007
10.6	0.558	0.817	0.224
11.0	0.522	0.764	0.309
11.5	0.235	0.344	1.906
12.0	0.047	0.069	13.572

References

1. E. Trepman and R. F. Chen, Fluorescence stopped-flow study of the o-phthaldialdehyde reaction, *Arch. Biochem. Biophys.*, 1980, **204**, 524-532.
2. O. S. Wong, L. A. Sternson and R. L. Schowen, Reaction of o-phthalaldehyde with alanine and thiols: kinetics and mechanism, *J. Am. Chem. Soc.*, 1985, **107**, 6421-6422.